A Molecular Orbital Study on the Reactivity of L-Ascorbic Acid towards OH Radical

Yasuo Abe,*[a] Satoshi Okada,[a] Ren Nakao,[a] Toyokazu Horii,[a] Hiroo Inoue,[a] Setsuo Taniguchi [b] and Shinichi Yamabe *[c]

[a] *Research Institute for Advanced Science and Technology, University of Osaka Prefecture, 1-2 Gakuen-cho, Sakai 593, Japan*

[b] *Faculty of Integrated Arts and Sciences, University of Osaka Prefecture, 1-1 Gakuen-cho, Sakai 593, Japan*

[c] *Department of Chemistry, Nara University of Education, Takabatake-cho, Nara 630, Japan*

The reaction between L-ascorbic acid (AAH_2) and OH radical has been investigated theoretically. The addition site on AAH_2 and AAH^- is found to be the olefinic carbon adjacent to the carbonyl group, with much more distinct selectivity for AAH^-. Dehydration is found to occur readily not from the neutral $^{\bullet}OH$ adduct $AAH_2OH^{\bullet}$, but from the anion adduct, $AAHOH^{\bullet -}$, which leads to formation of the most probable key intermediate radical **17** (ascorbate anion radical). The parent molecule of AAH_2, triose reductone TRH_2 (2,3-dihydroxyprop-2-enal), undergoes $^{\bullet}OH$ addition and dehydration in a similar manner to AAH_2. The addition site has been confirmed by comparison of MO energies for four possible transition states of the TRH_2 (*ab initio* and MNDO) and AAH_2 (MNDO) systems. The importance of the conjugate bases, AAH^- and TRH^-, for yielding the key radicals is suggested.

Redox and radiation-induced reactions of aqueous solutions of L-ascorbic acid (Vitamin C, called here AAH_2, **10**) have been extensively studied.[1] AAH_2 is readily oxidized to give a stable and unreactive radical $AAH^{\bullet}$. Owing to this characteristic, AAH_2 is relatively non-toxic and is useful as an anti-oxidant in biological systems. In radiation chemistry, formation of $AAH_2OH^{\bullet}$ has also been proposed. Through the use of pulse radiolysis and EPR spectroscopy (or spectrophotometry), the early stage of the radiation-induced reaction of AAH_2 has been investigated.[2,3] The experiment showed that the OH-radical adduct ($AAH_2OH^{\bullet}$) as well as $AAH^{\bullet}$ was generated.

The parent molecule with the enediol group is triose reductone (2,3-dihydroxyprop-2-enal, TRH_2, **1**). In our previous work,[4–6] oxidation reactions of TRH_2 were studied, and reactivity similar to that of AAH_2 was found. Pulse radiolysis of TRH_2 was also carried out, and the intermediate radical was traced by spectrophotometry.[7] The observed radical has the same λ_{max} (398 nm) as the one-electron oxidized radical ($TR^{\bullet -}$) and a pK value (4.7) different from that (1.4) of the latter radical. According to these data, the former radical was thought to be one of the OH-adduct radicals **3**–**6** in Scheme 1, however,

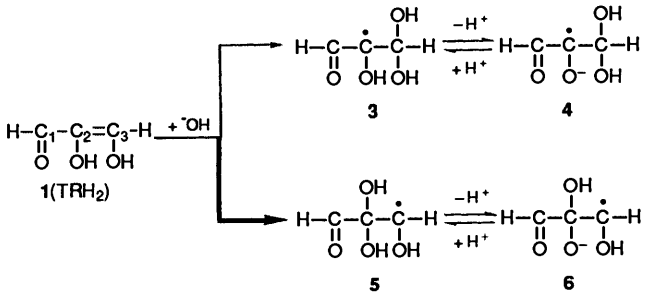

Scheme 1

the discussion was rather speculative. For instance, the site of the $^{\bullet}OH$ addition was suggested to be C2 of TRH_2 according to its higher electron density (not **3** but **5** formed).[8]

Through time-resolved EPR measurements, Fessenden detected radicals in the pulse radiolysis of AAH_2,[2,3] and identified two adduct radicals, **12** and **14**, and the one-electron oxidized radical **17** (Scheme 2). It was suggested that the radical **17** is generated from the AAH_2 tautomer, **10′**, but, the mechanism of $^{\bullet}OH$ addition and dehydration was reported to be complex and unclarified. For example, the pH dependence of radical formation has not yet been interpreted. In Scheme 2, broken arrows

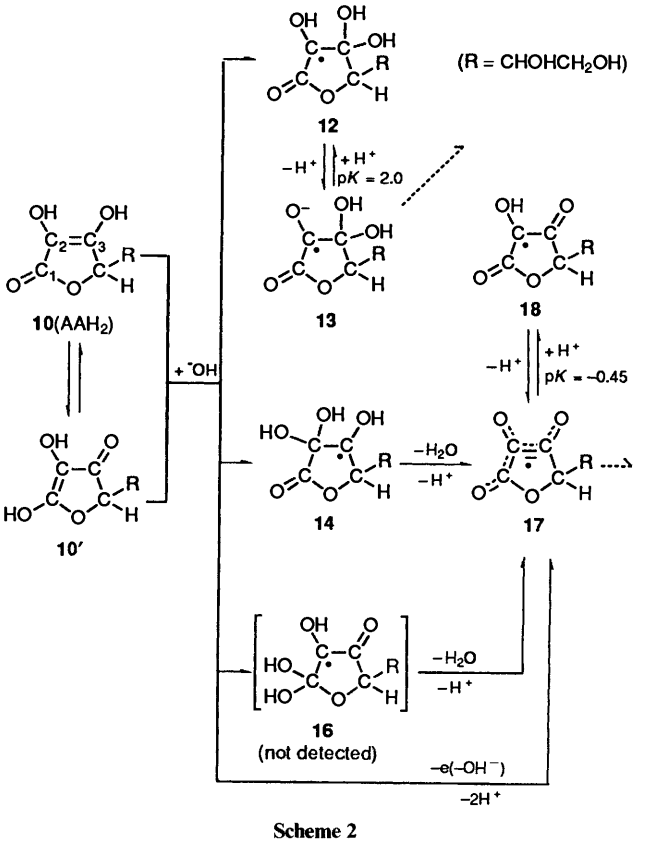

Scheme 2

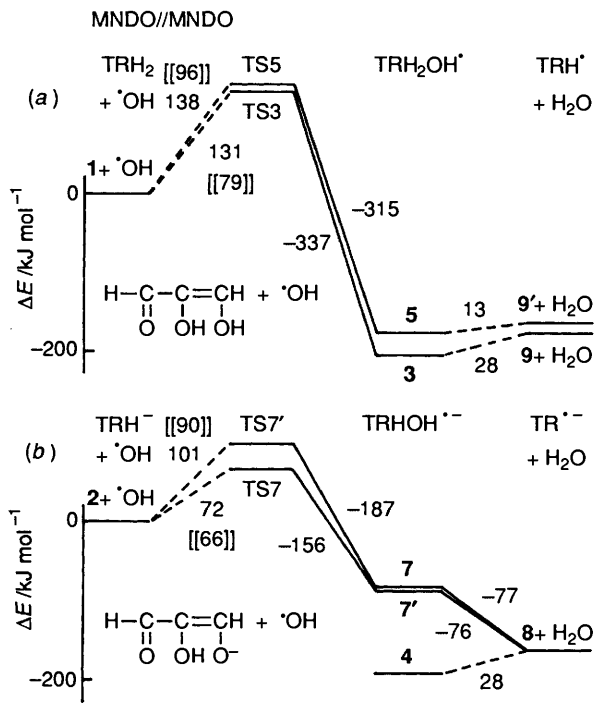

Fig. 1 Energy diagrams (by Method 2) of •OH addition to, and subsequent dehydration of, substrates, (*a*) TRH_2 and (*b*) TRH^-. Negative energies in kJ mol^{-1} show that the processes are exothermic. Total energies from Method 2 are given in Appendix B. Each species except the TSs is defined in Schemes 1 and 3. Activation energies in double brackets are those of CI = 6/MNDO.

starting from **13** and **17** denote radical terminations such as recombination and disproportionation.

In this work, these unclear mechanisms, and reactivities of the OH radical toward the enediol group in TRH_2 and AAH_2 were examined using molecular orbital (MO) calculations. Three main subjects are dealt with theoretically. (1) How is the site of the •OH addition to the enediol group determined? (2) How does dehydration of the •OH adduct occur? (3) Which radical is detected spectrometrically?

It is also of biological interest to examine the processes by which the toxic OH radical is trapped by Vitamin C in the body.

Method of Calculation

Optimizations of equilibrium and transition-state (TS) geometries were carried out with the MNDO semiempirical MO method developed by Dewar and Thiel[9a] in Method 1, *vide infra*. MNDO total energies were recalculated in Method 2.

Method 1. Optimizations were made with the AMPAC program.[10a] For radicals, the UHF scheme was used.

Method 2. For closed-shell molecules, energies are the same as those of Method 1. For radicals, single-point RHF HE calculations were made on the geometries of Method 1.[11]

Method 3. Optimizations with the 3-21G basis set using the GAUSSIAN 86 program[12] were performed on the TRH_2-group geometries. Subsequently, single-point calculations were made [for closed-shell molecules RHF/3-21(+)G//RHF/3-21G and for radicals ROHF/3-21(+)G//UHF/3-21G]. In the 3-21(+)G basis set, the diffuse sp GTOs[13] are added to the oxygen 3-21G. Single-point restricted calculations in Methods 2 and 3 are due to spin contamination in UHF S^2.

Optimized geometries of Methods 1 and 3 are displayed in Appendices A-1 to A-6.[14] Total energies from Methods 1, 2 and 3 are given in Appendix B. PM3[9b] and CI calculations were made with the MOPAC program.[10b]

Results

Site of the •OH Addition.—In order to determine the •OH addition site, activation energies for addition to TRH_2 (*a*) and to TRH^- (*b*) are compared in Figs. 1 and 2. Fig. 1 shows the MNDO energies, and Fig. 2 the *ab initio* energies. Fig. 3 demonstrates that the obtained geometries are really of transition states. For **1**, the activation energy of TS3 leading to the C3 adduct **3** is smaller than that of TS5 to the C2 adduct **5** by both Method 2 in Fig. 1(*a*) and Method 3 in Fig. 2(*a*). For **2**, on the contrary, the path leading to the C2 adduct **7** is more favourable than that to the C3 adduct, **7'** in Figs. 1(*b*) and 2(*b*). These activation energies indicate that TRH_2 and TRH^- behave differently in radical additions. Schemes 1 and 2 must be revised to consider the conjugate bases. Here, a new scheme (Scheme 3) is presented for TRH_2 and TRH^-. There are two different •OH-addition routes, **1** ⟶ **3** and **2** ⟶ **7**.

In contrast to the different orientation above, $TRH_2OH^•$ on C2 *vs.* $TRHOH^{•-}$ on C3, the OH radical attacks C2 of both AAH_2 and AAH^- in Fig. 4. For AAH_2 and AAH^-, two routes

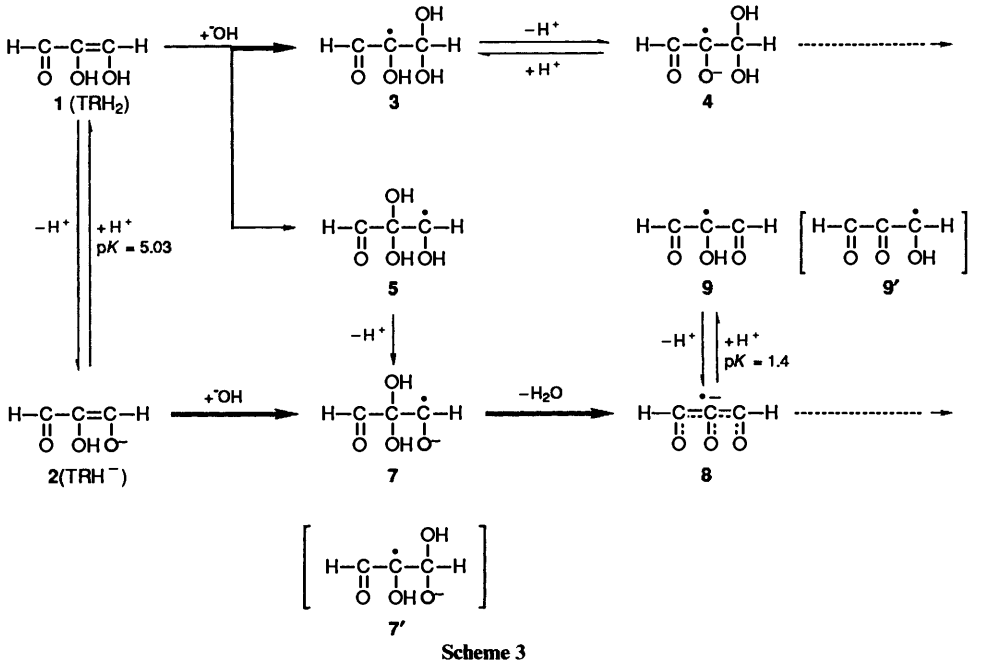

Scheme 3

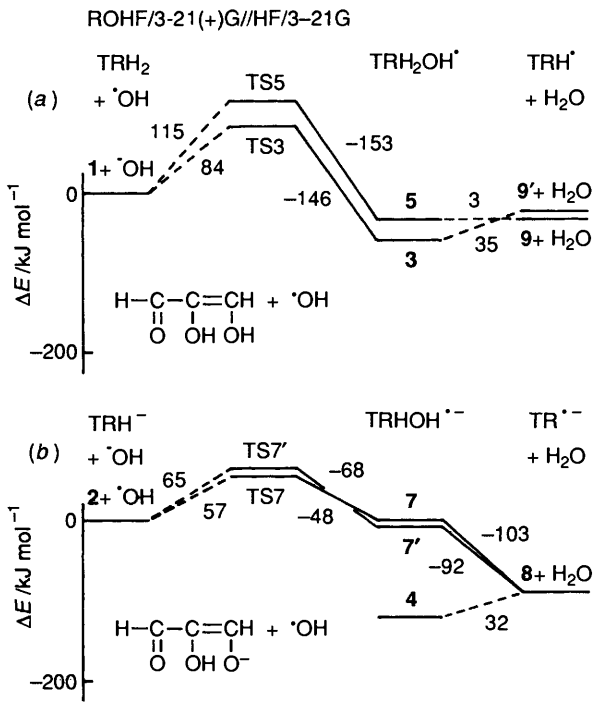

Fig. 2 Energy diagrams (by Method 3) of *ab initio* calculations. Notations are the same as those in Fig. 1

are drawn in Scheme 4. Since the OH radical is, by nature, an electrophilic reagent, the route starting from **11** is evidently dominant, with smaller activation energies. Geometries of obtained MNDO TSs are shown in Fig. 5. It is found that the OH radical attacks the C2 atom at the back side of the sidechain alkyl group (steric effect).

In the observed EPR data,[3] only **17** is trapped among anion radicals, while both neutral adducts **12** and **14** are detectable among neutral radicals. These data suggest that the site selectivity (C2 or C3) is more distinct in AAH^- than in AAH_2. Energy diagrams in Fig. 4 show this trend. While activation energies of TS12 and TS14 are similar, those of TS15 and TS15′ are quite different. In addition, the stability of **15** is much larger than that of **15′**. For the •OH-addition step, Figs. 1, 2 and 4 can be summarized as follows: MNDO and ROHF/3-21(+)G favour the conjugate base pathway (*b*) kinetically at the C2 site of TRH^- and AAH^-. This site selectivity is explicable in terms of frontier-orbital theory.[15] For the electrophilic reagent •OH, the HOMOs of AAH_2 and AAH^- are frontier orbitals. The difference in these shapes is consistent with the computed energies.

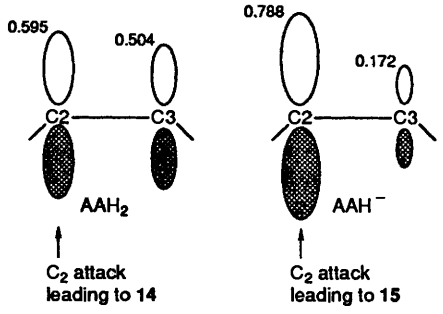

The effect of solvent on TS energies was examined by including four water molecules into TS3, TS5, TS7 and TS7′. First, the MNDO optimization was tested, resulting in the well-known overestimate of hydrogen-bond lengths. Second, PM3 optimization was performed to give TS geometries with four waters, shown in Fig. 3. In the (TS + $4H_2O$) scheme, the (TS3 − TS5) energy difference is 10 kJ mol^{-1} at RHF/PM3//UHF/PM3, and (TS7′ − TS7) is 6 kJ mol^{-1}. Thus, although activation energies are somewhat affected by the inclusion of water molecules, the energetic trend is the same as that in Fig. 1.

The electron correlation effect on activation energies was examined with configuration interaction (CI = 6 in the MOPAC keyword, CI/MNDO//UHF/MNDO). In Figs. 1 and 4, these energies are shown in double brackets and demonstrate that the energy order of TS5 > TS3, TS7′ > TS7,

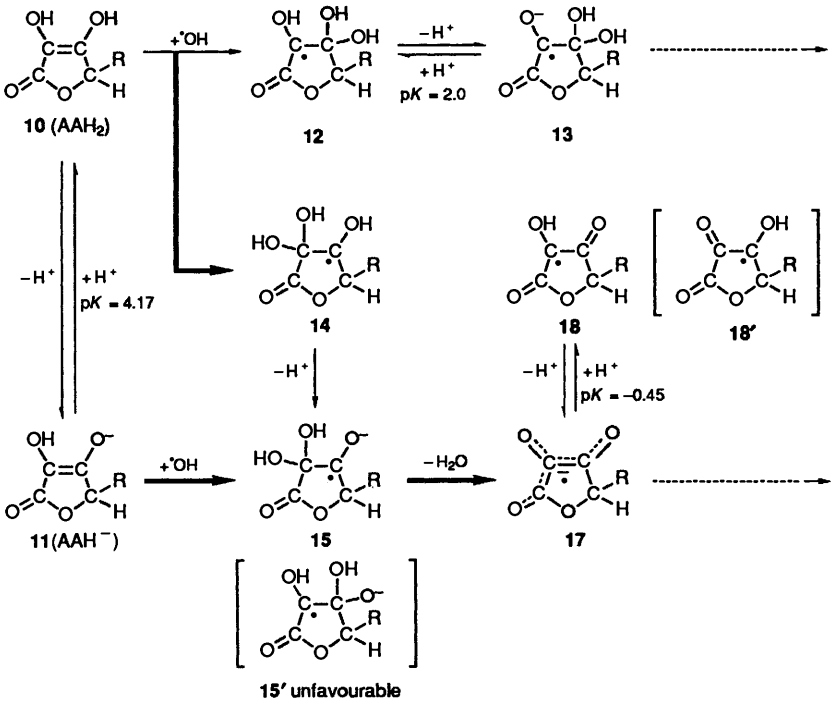

Scheme 4

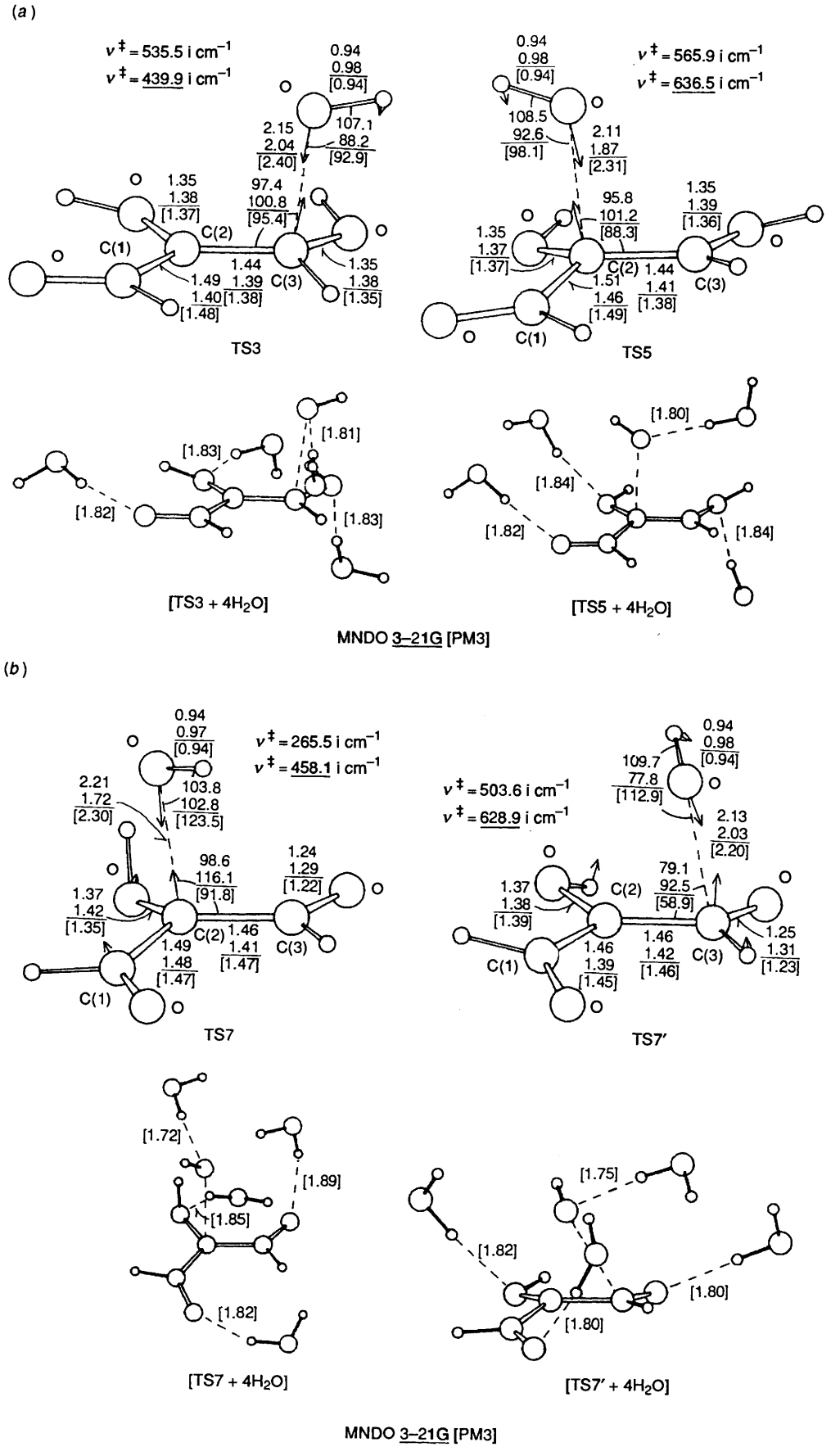

Fig. 3 MNDO and 3-21G geometries and sole imaginary frequencies ($\nu^{\ddagger}$) corresponding to transition states of the OH addition to TRH_2 (*a*) and to TRH^- (*b*). PM3 data with four water molecules are shown in brackets. Bond distances are in ångströms and angles are in degrees. Total energies of RHF/PM3//UHF/PM3 are −2904.445 64 (TS3 + $4H_2O$), −2904.342 43 (TS5 + $4H_2O$), −2892.722 46 (TS7 + $4H_2O$) and −2892.655 37 (TS7′ + $4H_2O$), respectively.

TS12 > TS14 and TS15′ > TS15 is the same as that of the Hartree–Fock calculation. It is noteworthy that four activation energies are lowered by inclusion of correlation effects, and accordingly the effect renders the present reacting system more realistic.

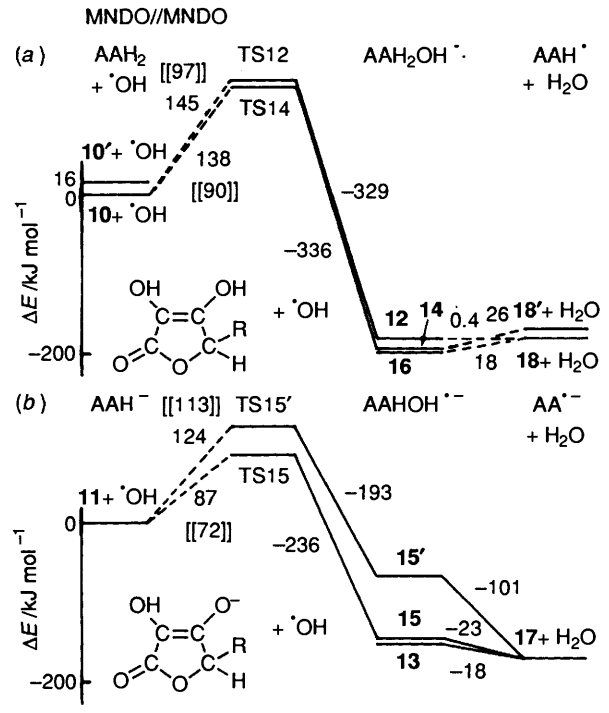

Fig. 4 Energy diagrams (by Method 2) on substrates, (*a*) AAH_2 and (*b*) AAH^-. Total energies from Method 2 are given in Appendix B. Each species except the TSs is defined in Schemes 2 and 4. Activation energies in double brackets are those of CI = 6/MNDO.

Dehydration of the OH Adduct.—Through OH attachment to the enediol group, a geminal dihydroxy group is formed. This group is known to be readily converted to the carbonyl group by loss of water.[16] Thus, a mechanistic question arises: which •OH adduct is more easily dehydrated, $TRH_2OH^•$ (the C3 adduct) or $TRHOH^{•-}$ (the C2 adduct)? Energy profiles for •OH addition and dehydration are shown in Figs. 1 and 2. When the OH-radical adduct **3** is dehydrated, **9** is formed. However, the process **3** ⟶ **9** is calculated to be +28 kJ mol^{-1} (MNDO), and +35 kJ mol^{-1} [3-21(+)G] endothermic.

For the conjugate base, TRH^-, the OH-radical adduct **7** is calculated to give **8** and H_2O exothermically [−77 kJ mol^{-1} (MNDO), −103 kJ mol^{-1} (3-21(+)G)]. Thus, in Scheme 3, the route **2** ⟶ **7** ⟶ **8** occurs readily. The result of difficult dehydration of **3** and facile one of **7** may be checked by a different calculation. Dehydration obviously occurs at the geminal OH groups through the following double proton migration.

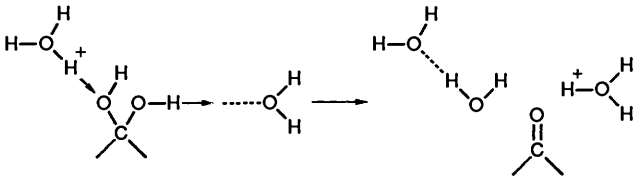

To simulate this process, geometries of protonated species $3H^+$ and $7H^+$ were optimized with MNDO UHF. A stable intermediate $3H^+$ is obtained.

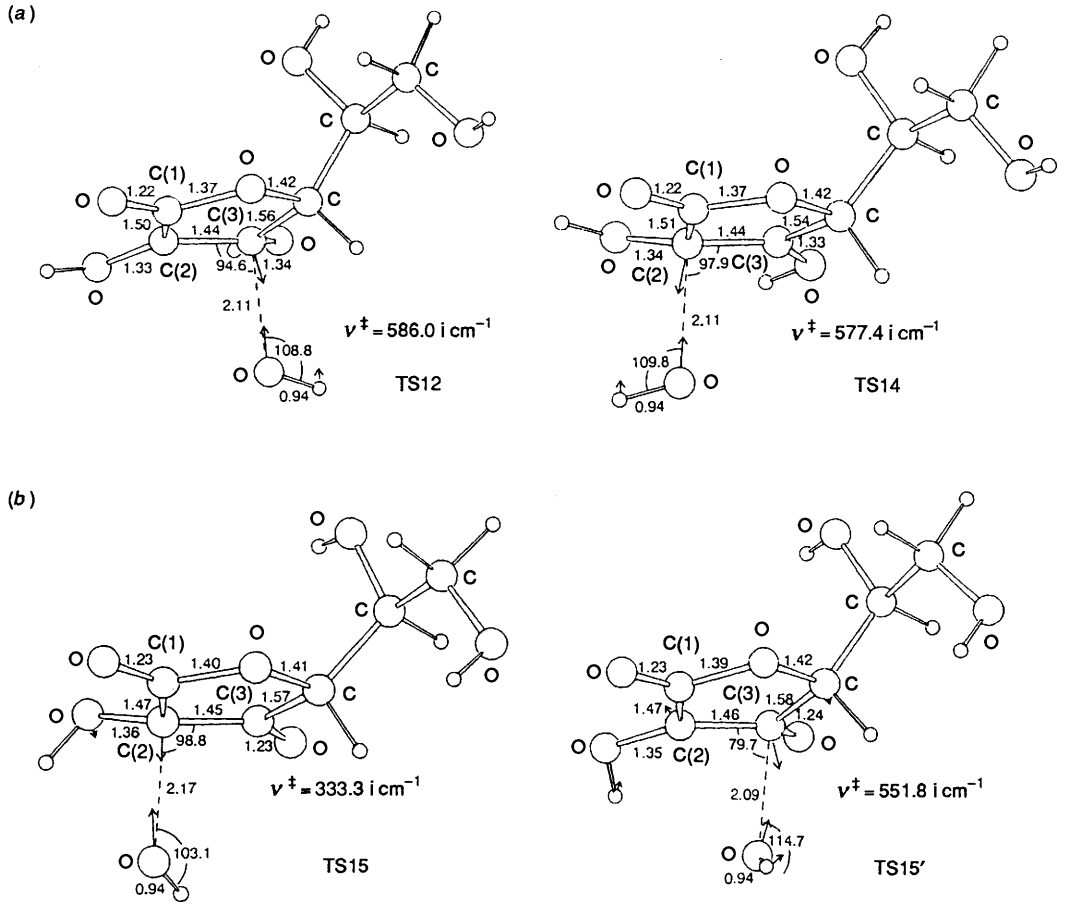

Fig. 5 MNDO TS geometries and sole imaginary frequencies of •OH addition to AAH_2 (*a*) and AAH^- (*b*)

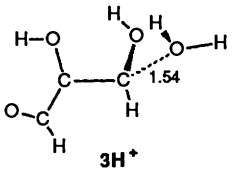

3H$^+$

On the other hand, protonated **7** dehydrates smoothly (without a significant energy barrier) to give **9** and H_2O.

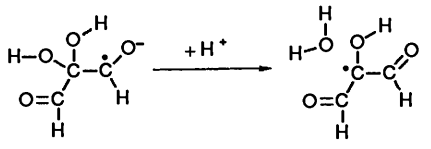

7 **9** + H_2O

That is, not **3** but **7** undergoes facile dehydration. Energy profiles for $^{\bullet}OH$ addition and dehydration of AAH_2 and AAH^- are shown in Fig. 4. The tautomer of AAH_2, **10′** (in Scheme 2) is calculated to be +16 kJ mol^{-1} unstable relative to **10**. In Fig. 4(*a*), dehydration from the neutral radical **12** does not proceed exothermically (**12** ⟶ **18** + H_2O), which is similar to the case of $TRH_2OH^{\bullet}$. On the other hand, the anion radical $AAHOH^{\bullet -}$ **15** proceeds smoothly to (**17** + H_2O) in Fig. 4(*b*).*

A noticeable result obtained here is that the *key* intermediate radical **17** is derived mainly from the base **15** rather than neutral adducts **12** and **14** in Scheme 4.

Detection of Intermediate Radicals.—In this subsection, spectrometric data reported so far are interpreted in terms of the computed data. First, **17** and **18** are discussed. The *key* radical **17** together with its protonated species **18** was observed immediately (*ca.* 2 μs) after the pulse irradiation. These radicals have large EPR signal intensities. Based on this rapid formation, **17** and **18** were thought to be generated by direct oxidation.[2,3] However, both AAH_2 (**10**) and the base AAH^- (**11**) are calculated to undergo direct electron-transfer with high endothermicity.† The direct oxidation route to **17** is thus ruled out, and the primary step of the reaction between AAH_2 (or AAH^-) and $^{\bullet}OH$ is confirmed to be the addition.

10 + $^{\bullet}OH$ ⟶ $AAH_2^{\bullet +}$ + OH^- ΔH_r = +1013 kJ mol^{-1}

11 + $^{\bullet}OH$ ⟶ **18** + OH^- ΔH_r = +244 kJ mol^{-1}

In the previous subsection, it was postulated that the major route is **11** ⟶ **15** ⟶ **17** in Scheme 4. Fessenden suggested that the route **10** ⟶ **14** ⟶ **17** is dominant in Scheme 2, where a large EPR intensity due to **17** and the small one due to **14** were observed.[3] Also, he proposed the structural formula **12** as the $^{\bullet}OH$ adduct (on C3) based on the EPR data. The EPR result of [**12**] > [**14**] appears to be inconsistent with our computed stability order **14** > **12** and the FMO prediction for AAH_2. However, **14** is rapidly converted to **17** in a 'bypass' *via* an unstable species **15**.

Principally, [**12**] < [**14**].

However, [**12**] > [**14**]. Because, **14** ⟶ **15** ⟶ **17**.

In Scheme 2, **16**, derived from the tautomer **10′** of AAH_2, has been shown, although its EPR signal was not observed. The absence of **16** was ascribed to its rapid dehydration (plus deprotonation) to give **17**.‡ However, this route (**16** ⟶ **18** + H_2O) has been calculated to be endothermic (+18 kJ mol^{-1}) in Fig. 4(*a*), and the route is found to be unfavourable.§

Conclusions

In this work, the reactivity of the enediol group toward the OH radical has been studied theoretically. AAH_2 and its parent molecule TRH_2 are found to have similar energetics in the $^{\bullet}OH$ addition and dehydration. It has been found that the *key* radical **17** $AA^{\bullet -}$ is formed by the route **11** ⟶ **15** ⟶ **17**. The conjugate base **11**, which was not considered previously,[2,3] is a dominant precursor.

Answers to the three questions addressed in the Introduction may be offered here.

(1) The most probable $^{\bullet}OH$ addition to the enediol group is **11** (AAH^-) + $^{\bullet}OH$ ⟶ **15**.

(2) Dehydration may take place from **15** through a double proton transfer process.

(3) The *key* radical is confirmed to be **17** $AA^{\bullet -}$ (or **8** $TR^{\bullet -}$). The neutral adducts **12** and **14** are also detectable, since these species do not undergo dehydration. A 'bypass' route **14** ⟶ **15** ⟶ **17** decreases the concentration of **14**.

Direct electron transfer (*e.g.*, AAH_2 ⟶ $AAH_2^{\bullet +}$ + e^-) is unlikely, when no oxidative reagents, such as metal ions, other than the OH radical are present.

Acknowledgements

The authors wish to thank the Data Processing Centre of Kyoto University for allotment of the CPU time on the FACOM M-780 computer. Thanks are also due to the Institute for Molecular Science for use of the HITAC M-680H computer and

* An independent dehydration route **13** ⟶ **17** + H_2O appears to be likely in view of its exothermicity, −18 kJ mol^{-1} [Fig. 4(*b*)]. However, this route has been ruled out spectroscopically. See refs. 2 and 3. **13** has been shown to intervene on the τ = 100 μs time scale. One possibility for this discrepancy would be that the freely rotating alkyl sidechain blocks the approach of H_3O^+ towards geminal hydroxy groups (hydrophobic effect).

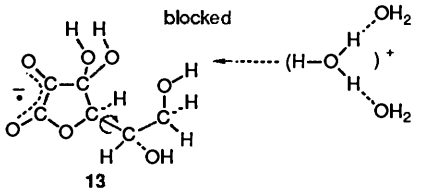

13

† The direct electron-transfer reaction is not always endothermic with the present method. For instance, while for TRH^- + $^{\bullet}OH$ ⟶ $TRH^{\bullet}$ + OH^- ΔH_r = +184 kJ mol^{-1}, for TR^{2-} + $^{\bullet}OH$ ⟶ $TR^{\bullet -}$ + OH^- ΔH_r = −484 kJ mol^{-1}. The dianion TR^{2-} undergoes the exothermic reaction.

‡ The EPR intensity of **17** (or **18**) depended on the pH, and was a maximum at pH *ca.* 6.7. It is natural that in acidic solution the concentration of **17** is small, because that of the precursor (conjugate base **11**) is small. It seems to be strange that in alkaline solution the intensity becomes decreased. This decrease would be attributed to the increased probability of S_N2 reactions of the hydroxide ion.

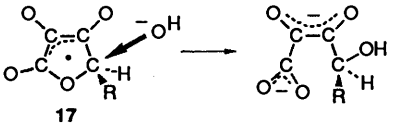

17

§ The absence of **16** comes probably from two sources. One is in the unfavourable tautomerism **10** ⇌ **10′**. The MNDO calculation has given the 16 kJ mol^{-1} energy difference between **10** and **10′** in Fig. 4(*a*). The other source is the peculiar bonding at the C1 of **16**. C1 is bonded to three oxygen atoms, which makes **16** undergo reactions (*e.g.* ring opening by scission of the C–O bond) other than hydration.

to the Information Processing Centre of Nara University of Education for use of the CONVEX C-220 computer. The present research is supported in part by Grant-in-Aid for Scientific Research on Priority Area, 'Theory of Chemical Reactions', from the Ministry of Education, Science and Culture.

References

1 B. H. J. Bielski, *Ascorbic Acid: Chemistry, Metabolism, and Uses*, eds. P. A. Seib and B. M. Tolbert, ACS Adv. in Chem. Ser. No. 200, Washington, 1982, pp. 81–100 and references therein.
2 G. P. Laroff, R. W. Fessenden and R. H. Schuler, *J. Am. Chem. Soc.*, 1972, **94**, 9062.
3 R. W. Fessenden and N. C. Verma, *Proceedings of Meeting on Fast Biochemical Reactions in Solutions, Membranes, and Cells*, Rockefeller University Press, New York, 1978, pp. 93–101 and references therein.
4 Y. Abe, H. Horii, S. Taniguchi, K. Kamai and M. Takagi, *Bull. Chem. Soc. Jpn.*, 1983, **56**, 467; Y. Abe, H. Horii and S. Taniguchi, *Bull. Chem. Soc. Jpn.*, 1984, **57**, 222; Y. Abe, T. Dohmaru, H. Horii and S. Taniguchi, *Can. J. Chem.*, 1985, **63**, 1005.
5 H. Horii, Y. Abe and S. Taniguchi, *Bull. Chem. Soc. Jpn.*, 1985, **58**, 2751.
6 Y. Abe, H. Horii, S. Taniguchi, S. Yamabe and T. Minato, *Can. J. Chem.*, 1986, **64**, 360.
7 H. Horii, Y. Abe and S. Taniguchi, *Bull. Chem. Soc. Jpn.*, 1986, **59**, 721.
8 J. K. Kochi, *Free Radicals*, ed. J. K. Kochi, John Wiley, New York, 1973, vol. 2, p. 672.
9 (*a*) M. J. S. Dewar and W. Thiel, *J. Am. Chem. Soc.*, 1977, **99**, 4899; (*b*) J. J. P. Stewart, *J. Comput. Chem.*, 1989, **10**, 209.
10 (*a*) AMPAC, QCPE No. 523. Department of Chemistry, Indiana University, Bloomington, Indiana, U.S.A.; (*b*) MOPAC (V. 5.0), QCPE No. 455.
11 T. Clark, *A Handbook of Computational Chemistry*, John Wiley, New York, 1985, p. 176.
12 M. J. Frisch, J. S. Binkley, H. B. Schlegel, K. Raghavachari, C. F. Melius, R. L. Martin, J. J. P. Stewart, F. W. Bobrowicz, C. M. Rohlfing, L. R. Kahn, D. J. Defrees, R. Seeger, R. A. Whiteside, D. J. Fox, E. M. Fleuder and J. A. Pople, GAUSSIAN 86; Carnegie-Mellon Quantum Chemistry Publishing Unit, Pittsburg, PA, 1984.
13 T. Clark, J. Chandrasekhar, G. Spitznagel and P. v. R. Schleyer, *J. Comput. Chem.*, 1983, **4**, 294.
14 For the STO-3G geometries of **10**, **11**, **17** and **18**, see Y. Abe, S. Okada, H. Horii, S. Taniguchi and S. Yamabe, *J. Chem. Soc., Perkin Trans. 2*, 1987, 715; M. A. Al-Laham and G. A. Petersson, *J. Comput. Chem.*, 1991, **11**, 113.
15 K. Fukui, *Theory of Orientation and Stereoselection*, Springer Verlag, Berlin, 1970.
16 P. Salomaa, *The Chemistry of the Carbonyl Group*, ed. S. Patai, Interscience, London, 1966, pp. 177–179.
17 D. Semmingsen, *Acta Chem. Scand., Ser. B*, 1974, **28**, 141.
18 J. Hvoslev, *Acta Crystallogr., Sect. B*, 1968, **24**, 23.
19 J. Hvoslev, *Acta Crystallogr., Sect. B*, 1969, **25**, 2214.

Paper 2/02959F
Received 5*th June* 1992
Accepted 12*th August* 1992

Appendix

Calculated equilibrium geometries are shown in Appendices A1–A6. In A1–A3, the 3-21G RHF or UHF data (Method 3) are shown by italic numbers.

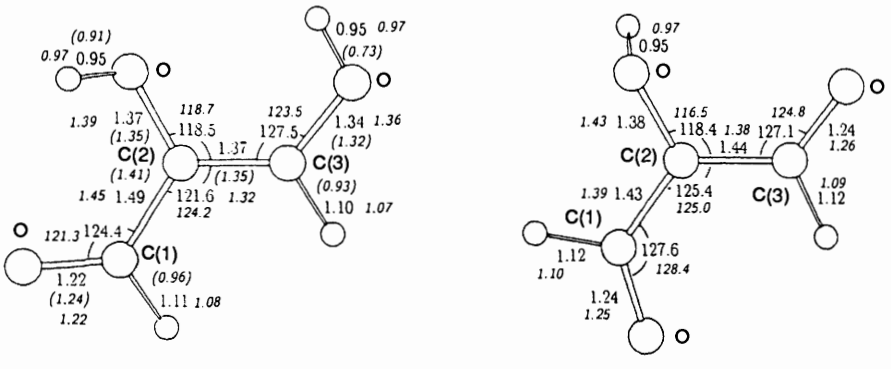

1(TRH$_2$) 2(TRH$^-$)

Appendix A1 MNDO-optimized (Method 1) geometries of 2,3-dihydroxyprop-2-enal (TRH$_2$, **1**) and its conjugate base (**2**). These are planar molecules. Empty circles denote hydrogen atoms. Distances are in angstrom and angles are in degrees. Numbers in parentheses of **1** stand for X-ray data.[17]

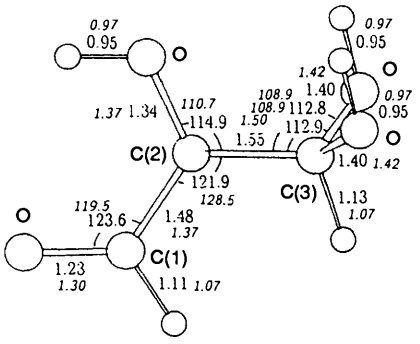

3($TRH_2OH^{\bullet}$)

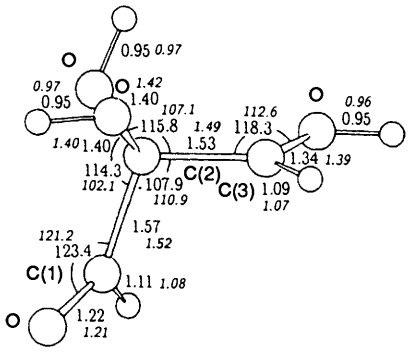

5($TRH_2OH^{\bullet}$)

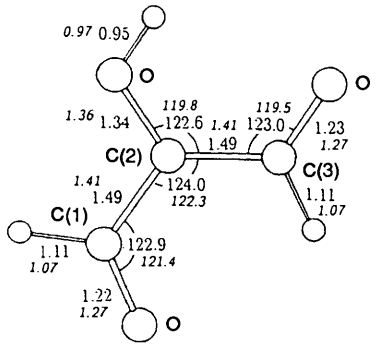

9($TRH^{\bullet}$)

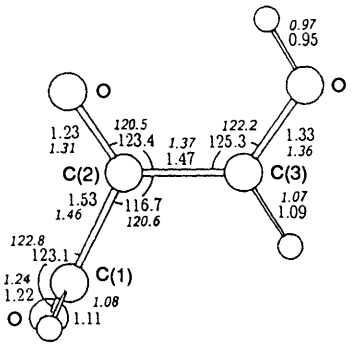

9′($TRH^{\bullet}$)

Appendix A2 MNDO geometries of TRH_2OH adduct radicals and TRH radical

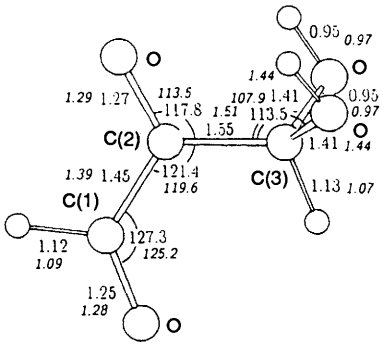

4($TRHOH^{\bullet -}$)

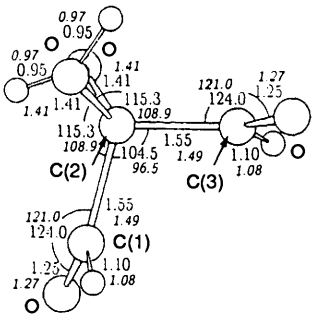

7($TRHOH^{\bullet -}$)

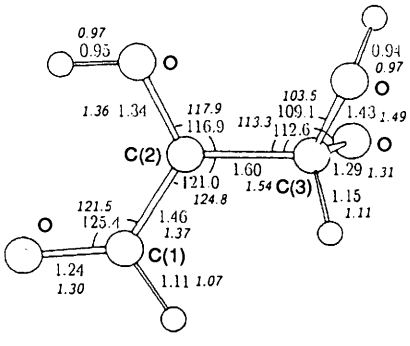

7′($TRHOH^{\bullet -}$)

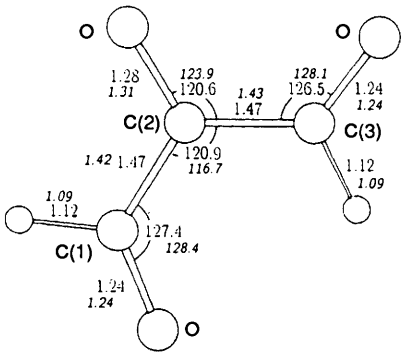

8($TR^{\bullet -}$)

Appendix A3 MNDO geometries of anion radicals

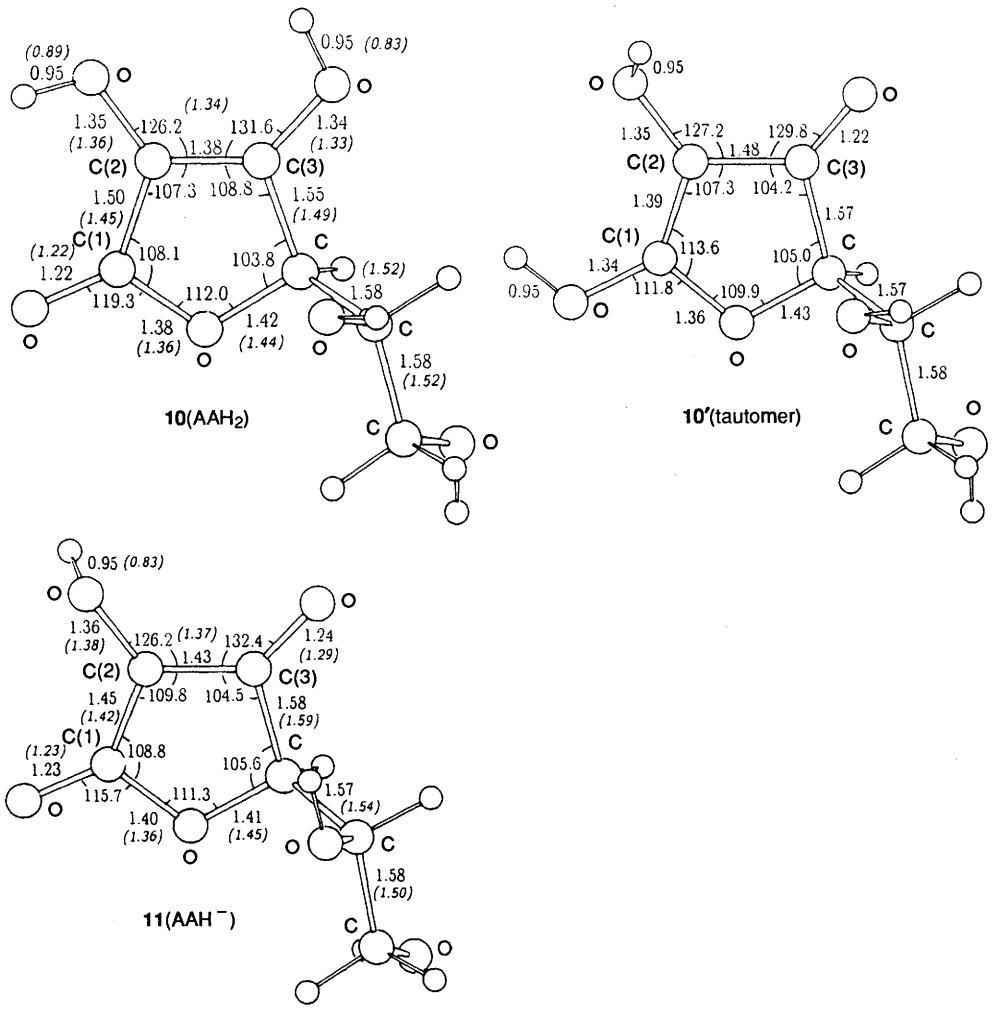

Appendix A4 MNDO-optimized geometries of L-ascorbic acid (**10**), its tautomer (**10′**) and its conjugate base (**11**). For **10** and **11**, the X-ray data are shown in parentheses.[18,19]

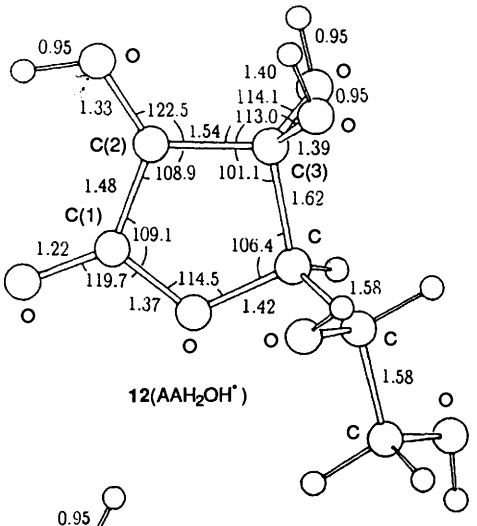

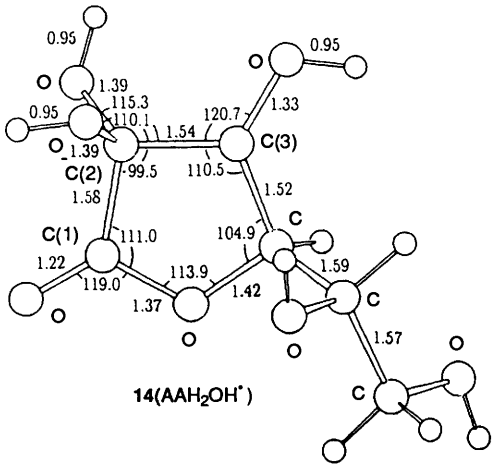

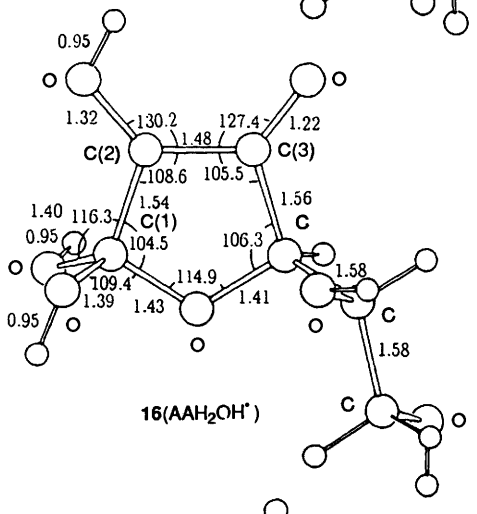

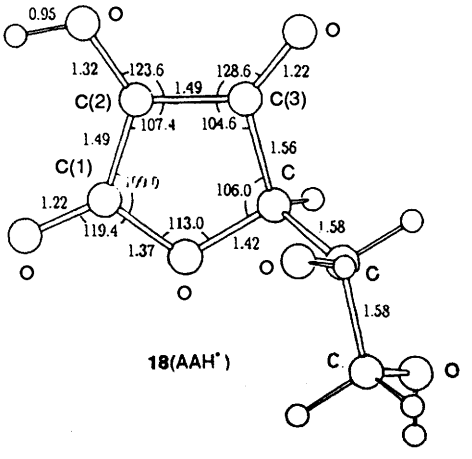

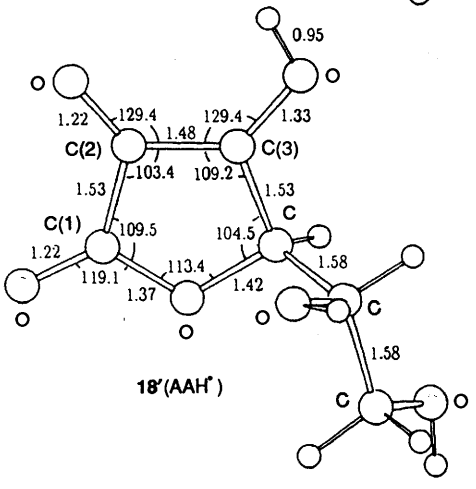

Appendix A5 MNDO geometries of neutral radicals

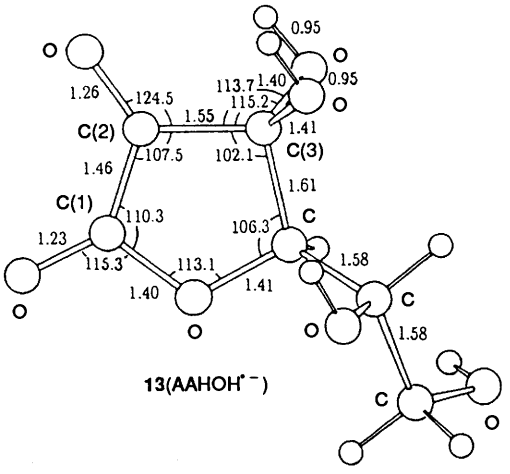

13(AAHOH$^{\bullet -}$)

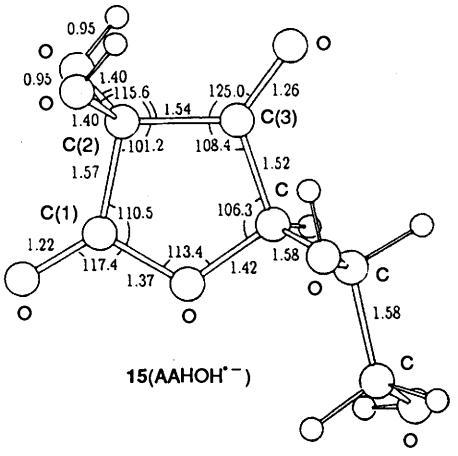

15(AAHOH$^{\bullet -}$)

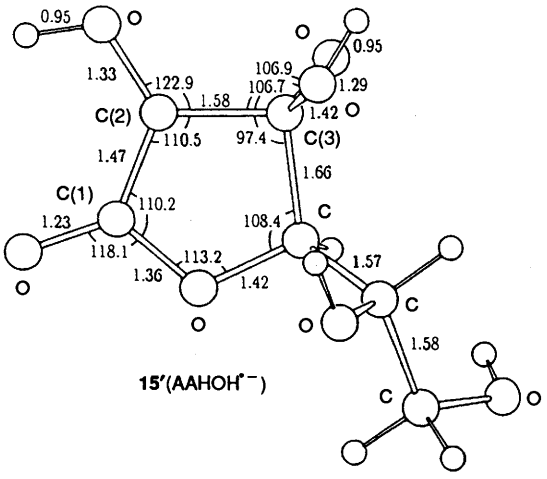

15′(AAHOH$^{\bullet -}$)

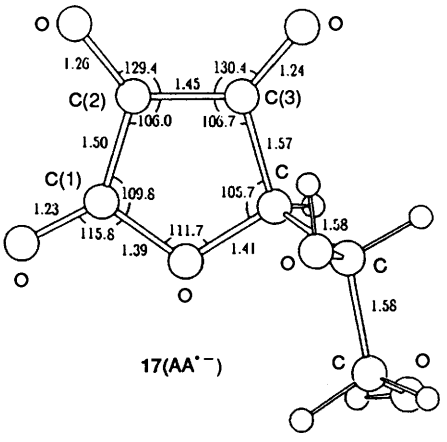

17(AA$^{\bullet -}$)

Appendix A6 MNDO geometries of anion radicals

Appendix B Total energies for MNDO (Method 1) and 3-21G (Method 3) optimized geometries given in Figs. 3 and 5 and Appendices A1–A6. Expectation values S^2 of the spin eigenfunction in UHF calculations are shown in parentheses for Methods 1 and 3

	Species	Formula		Method 1[a] HF/MNDO/eV (S^2)	Method 2[b] RHF/MNDO/ eV	Method 3[c] 3-21(+)G/a.u. (S^2)
TRH_2	**1**	TRH_2	2,3-dihydroxyprop-2-enal	−1406.825 51	−1406.825 51	−338.636 80
	2	TRH^-	conjugate base of **1**	−1394.007 36	−1394.007 36	−338.097 18
	3	$TRH_2OH^•$	C3-adduct	−1743.695 08 (0.77)	−1743.549 15	−413.656 13 (0.95)
	4	$TRHOH^{•-}$	conjugate base of **3**	−1730.669 48 (0.78)	−1730.570 35	−413.140 60 (0.84)
	5	$TRH_2OH^•$	C2-adduct	−1743.343 43 (0.76)	−1743.256 32	−413.646 68 (0.77)
	7	$TRHOH^{•-}$	conjugate base of **5**	−1729.582 00 (0.76)	−1729.480 12	−413.089 13 (0.83)
	7′	$TRHOH^{•-}$	C3-adduct	−1729.638 41 (0.78)	−1729.495 74	−413.093 70 (0.86)
	8	$TR^{•-}$	anion radical	−1379.053 85 (0.78)	−1378.854 49	−337.509 48 (0.84)
	9	$TRH^•$	acid of **8** (C2-OH)	−1392.002 73 (0.78)	−1391.833 13	−338.023 62 (1.23)
	9′	$TRH^•$	acid of **8** (C3-OH)	−1391.856 35 (0.78)	−1391.701 79	−338.026 40 (1.19)
	TS3		TS for **3**	−1740.914 22 (1.21)	−1740.057 08	−413.600 25 (1.38)
	TS5		TS for **5**	−1740.757 07 (1.19)	−1739.989 04	−413.588 46 (1.25)
	TS7		TS for **7**	−1728.117 86 (0.75)	−1727.858 88	−413.070 85 (0.83)
	TS7′		TS for **7′**	−1727.783 42 (0.85)	−1727.553 53	−413.067 92 (1.23)
		$^•OH$		−334.606 82 (0.75)	−334.594 71	−74.995 37 (0.75)
		H_2O		−351.424 83	−351.424 83	−75.619 04
		OH^-		−334.867 11	−334.867 11	
AAH_2	**10**	AAH_2	L-ascorbic acid	−2814.376 39	−2814.376 39	
	10′	AAH_2	tautomer of **10**	−2814.208 30	−2814.208 30	
	11	AAH^-	conjugate base of **10**	−2802.125 92	−2802.125 92	
	12	$AAH_2OH^•$	C3-adduct	−3151.011 77 (0.77)	−3150.880 41	
	13	$AAHOH^{•-}$	conjugate base of **12**	−3138.471 63 (0.77)	−3138.311 14	
	14	$AAH_2OH^•$	C2-adduct	−3151.113 27 (0.76)	−3151.018 70	
	15	$AAHOH^{•-}$	conjugate base of **14**	−3138.405 89 (0.75)	−3138.258 47	
	15′	$AAHOH^{•-}$	C3-adduct to **11**	−3137.605 68 (0.77)	−3137.443 07	
	16	$AAH_2OH^•$	C1-adduct to **10′**	−3151.206 64 (0.77)	−3151.057 76	
	17	$AA^{•-}$	anion radical	−2787.256 31 (0.80)	−2787.067 58	
	18	$AAH^•$	acid of **17** (C2-OH)	−2799.613 72 (0.78)	−2799.448 15	
	18′	$AAH^•$	acid of **17** (C3-OH)	−2799.494 57 (0.78)	−2799.320 57	
		$AAH_2^{•+}$		−2815.964 72 (0.76)	−2803.600 32	
	TS12		TS for **12**	−3148.291 29 (1.23)	−3147.467 49	
	TS14		TS for **14**	−3148.341 77 (1.21)	−3147.539 72	
	TS15		TS for **15**	−3136.128 45 (0.76)	−3135.814 32	
	TS15′		TS for **15′**	−3135.677 46 (0.89)	−3135.439 07	
	TS16		TS for **16**	−3148.034 27 (1.02)	−3147.437 11	
	TS16B		TS for **16**	−3148.067 22 (1.19)	−3147.264 74	

[a] MNDO OPT of the AMPAC program in ref. 10. Radicals are treated by the UHF method. [b] For radicals optimized in Method 1, single-point HE energy calculations are made. For closed-shell molecules, Method 1 = Method 2. [c] ROHF/3-21(+)G//HF/3-21G. (S^2) is of UHF/3-21G.